SCIEPublish

*Article*

# Experimental Study on A Novel Organic/Inorganic Green Deep Eutectic Solvents: Thermophysical Properties, Thermal Stability, and Utilization in Nanofluids

**Xiao Zhang [1], Xinqian Du [1], Jiahuan He [1], Pei Liu [1], Wenbo Huang [2], Guangyuan Liang [1], Haolin Gan [1], Jiateng Zhao [1] and Changhui Liu [1,*]**

[1] School of Low-Carbon Energy and Power Engineering, China University of Mining and Technology, Xuzhou 221116, China; 1661052363@qq.com (X.Z.); 2743432757@qq.com (X.D.); 3514001439@qq.com (J.H.); 2967303851@qq.com (P.L.); 1279155924@qq.com (G.L.); 769154741@qq.com (H.G.); zhaojiateng@cumt.edu.cn (J.Z.)

[2] Hubei Three Gorges Laboratory, Yichang 443007, China; 15527993205@163.com (W.H.)

* Corresponding author. E-mail: liuch915@cumt.edu.cn (C.L.)

Received: 21 January 2025; Accepted: 10 March 2025; Available online: 17 March 2025

**ABSTRACT:** In response to the performance limitations of traditional heat transfer fluids under extreme conditions, a series of organic/inorganic deep eutectic solvents (DES), composed of ethylene glycol and different types of acetates, have been developed, and their downstream thermophysical properties, as well as their potential applications in nanofluids, have been explored. It is found that the prepared DESs significantly broaden the liquid phase temperature range, which ranges from −14~196 °C to −40~201 °C. The initial decomposition temperature increases from 85 °C to 130 °C, and the peak decomposition rate shifts from 175 °C to 206 °C. Subsequently, nanofluids were prepared by employing the selected ethylene glycol: potassium acetate-5:1 DES with carbon nanotube as nanofiller. The results reveal that the thermal conductivity of the nanofluid could be increased by approximately 3% compared to the base fluid, and the specific heat capacity was enhanced by 7.5% with a photothermal conversion efficiency reaching up to 42.7%. These results highlight the promising thermal stability and heat transfer properties of ethylene glycol-acetate DESs. Moreover, the nanofluids prepared from those DESs as base fluids provide useful references for the development of novel, green, and high-efficiency energy transportation fluids.

**Keywords:** Deep eutectic solvents; Thermophysical properties; Thermal stability; Nanofluid; Photothermal conversion efficiency



## 1. Introduction

With the evolving global situation, the demand for energy continues to rise, while traditional fossil energy resources are dwindling, and environmental pollution issues are becoming increasingly severe. Consequently, improving energy efficiency, reducing environmental pollution, and developing clean energy have become common objectives for nations worldwide [1,2]. However, the current methods and technologies for energy utilization still face several challenges, such as low energy conversion efficiency, significant energy waste, and an irrational energy structure. These issues not only affect the security of energy supply but also exacerbate environmental pollution [3,4]. In this context, the development of new, efficient heat transfer fluids is particularly critical. Heat transfer fluids play a key role in energy conversion and utilization, and their performance directly influences both the efficiency of energy usage and the extent of environmental impact [5]. The development of new, high-efficiency heat transfer fluids can enhance energy conversion efficiency, reduce energy waste, and minimize environmental pollution, thereby contributing to the sustainable development of energy. Therefore, research and development of innovative and efficient heat transfer fluids are essential for advancing energy utilization technologies and providing effective solutions to energy and environmental challenges [6–8].

Deep eutectic solvents (DES) are a class of binary or multicomponent mixtures composed of a hydrogen bond donor (HBD), such as polyols, and a hydrogen bond acceptor (HBA), such as acids or salts. These solvents exhibit

melting points that are significantly lower than the melting points of their components, which is why they are referred to as "deep eutectic" [9]. While eutectic systems with significantly depressed melting points were identified in the late 1990s, the term "deep eutectic solvents" and their specific properties were first introduced and popularized by Abbott et al. in 2003, and the concept of DES itself has also evolved. In recent years, DESs have gained considerable attention due to their unique physicochemical properties, leading to a wide range of applications across various fields [10–14].

Due to their unique advantages, DESs have attracted significant attention as potential candidates for new heat transfer fluids. For example, DESs are typically made from natural or renewable components, which results in a lower environmental impact and makes them biodegradable [15,16]. Furthermore, DESs have low volatility, which can significantly reduce the exposure risks in workplaces and the atmosphere [17,18]. In addition, because DESs are often synthesized from inexpensive and renewable raw materials, their production costs are generally lower [19]. As a result, researchers have increasingly focused on investigating the thermophysical properties of DESs. Lim et al. [20] conducted a comparative study of the thermophysical properties of choline chloride-based DESs and imidazolium-based ionic liquids (ILs), with a focus on differences in thermal conductivity, viscosity, and ionic conductivity, as well as their underlying mechanisms. Their results revealed that the thermal conductivity of DESs increased with the proportion of the hydrogen bond donor (HBD). Viscosity, on the other hand, showed significant differences related to the donor type and proportion. In contrast, the thermal conductivity and viscosity of ILs were primarily influenced by the carbon chain length. Increasing temperature resulted in decreased viscosity and increased ionic conductivity, and the introduction of water further enhanced both the thermal conductivity and conductivity of the system while drastically reducing viscosity. This study demonstrated that DESs, with their excellent tunability, low cost, and environmental friendliness, could potentially serve as a green alternative to ILs. Halder et al. [21] utilized a large dataset of 145 types of DESs and 1154 data points, combined with external validation data, to construct a highly accurate linear model for predicting the density of DESs at varying compositions and temperatures. The study highlighted the significant impact of DESs molecular structure and composition on their density and underscored the importance of descriptors such as hydrogen bond donor-acceptor interactions, polarity, and topological characteristics. Li et al. [22] conducted an in-depth study on the viscosity of DESs using an XGBoost machine learning model combined with SHAP analysis. They compiled a dataset of 994 experimental viscosity values from 107 DESs, incorporating the effect of water content on viscosity. The study revealed that HBDs play a dominant role in viscosity, with long-chain structures and strong hydrogen bonding interactions increasing viscosity, while higher temperatures and water content contribute to viscosity reduction.

Based on the significant thermophysical properties and tunability of related characteristics, recent experimental studies have explored the use of DESs as base fluids for the preparation of nanofluids. Sun et al. [23] investigated a novel nanofluid prepared by adding $Fe_2O_3$ nanoparticles to a glycerol-triethylene glycol sodium acetate DESs solution. The experiments demonstrated that the glycerol/triethylene glycol sodium acetate DESs with a molar ratio of 2:1 reduced the viscosity by 58.03% and increased the thermal conductivity by 17.2% at 25 °C. Dehury et al. [24], using both experimental and machine learning approaches, explored the thermophysical properties of DESs and nanofluids doped with hexagonal boron nitride nanoparticles, including density, viscosity, thermal conductivity, and specific heat capacity. Using the COSMO-SAC model, they calculated the eutectic points of the DESs and optimized their compositions. Experimental testing was carried out to evaluate the stability and thermophysical properties of the nanofluids, while multiple machine learning models (such as Lasso regression, random forests, and support vector regression) were developed to predict thermophysical properties at varying compositions and temperatures. The study showed that adding a small amount of nanoparticles significantly enhanced the thermal conductivity and specific heat capacity of the nanofluid, while viscosity and density were less affected by temperature and concentration. Additionally, the machine learning models exhibited high prediction accuracy (with $R^2$ values exceeding 0.99), providing a reliable tool for future heat fluid design, although further experimental data is needed for supplementary support.

In medium-to-high temperature operating environments, thermal stability is crucial for the performance of working fluids, as it directly impacts system reliability and safety [25–27]. Good thermal stability ensures that the working fluid does not undergo thermal decomposition or degradation under high-temperature conditions, thereby maintaining the stability of its chemical and physical properties. This extends the service life of equipment, reduces maintenance costs, and plays a significant role in optimizing design, improving work efficiency, and ensuring safe system operation [28–32]. Al-Kayiem et al. [33] pointed out that traditional working fluids in industrial operations suffer from issues such as poor biocompatibility, volatility, and corrosiveness, whereas binary DESs can resolve these problems due to their unique properties. Using molecular dynamics simulations and experimental techniques, they studied the thermophysical properties, rheological characteristics, electrical conductivity, and thermal stability of 11 types of binary DESs as biocompatible working fluids. The results showed that most DESs exhibit good thermal stability below 150 °C, and

DESs based on zinc ions generally perform better, making them suitable for high-temperature heat transfer systems. Majid et al. [34] focused on exploring the impact of ethoxy repeat units in different ethylene glycol structures (ethylene glycol, triethylene glycol, and polyethylene glycol) on the thermal stability of DESs. The results demonstrated that thermal stability significantly improves with the increase in ethoxy chain length. Additionally, FTIR analysis confirmed the formation of hydrogen bonds in the DESs, indicating that the length of the ethoxy repeat unit not only affects the strength of intermolecular interactions but also determines the energy required for decomposition. Designing DESs with longer-chain hydrogen bond donors can achieve higher thermal stability. Marchel et al. [35] studied the thermal stability of three choline chloride-based DESs and their decomposition behavior and toxicity under high-temperature conditions, focusing on the limitations of thermal instability on the green solvent potential. The study found that the choice of HBD significantly influences the thermal stability of DESs. Among them, DESs with urea as the HBD exhibited the highest thermal stability, remaining stable after prolonged heating at 120 °C, with limited decomposition products and low toxicity. Mu et al. [36] systematically investigated the thermal stability of 40 DESs using thermogravimetric analysis (TGA). They found that their decomposition behavior differs from that of ionic liquids, exhibiting a progressive degradation process. The decomposition is initiated by the disruption of hydrogen bonds, followed by the breakdown of HBDs, while HBAs decompose at higher temperatures. The study highlights the crucial role of hydrogen bond strength in thermal stability, demonstrating that stronger hydrogen bonding increases the onset decomposition temperature of DESs.

DESs composed of ethylene glycol (EG) and choline chloride have been extensively studied and applied due to their low cost and good tunability. However, their thermal stability and environmental friendliness remain limited under extreme conditions. For example, choline chloride is prone to decomposition at high temperatures, releasing harmful gases such as ammonia and hydrogen chloride [37,38]. Valentina et al. [39] conducted an extensive molecular dynamics simulation study to investigate the structural properties of four DESs, including choline chloride-urea and its three analogs, where chloride was replaced by fluoride, nitrate, and acetate. The study revealed that the hydrogen bond acceptor strength of the anions followed the order: acetate > chloride > nitrate > fluoride, indicating that acetate is the strongest hydrogen bond acceptor among these anions, making it a promising candidate for better DESs combinations. Maria et al. [40] explored the structural changes of two DESs, choline chloride-urea, and acetate choline-urea, under gradual hydration conditions. Their findings showed that replacing chloride ions with acetate had a significant impact on the structure and dynamics of DESs. Under low moisture conditions, the DESs-DESs interactions began to break down, rapidly dissolving the urea portion and achieving a complete exchange of mobile protons. In contrast, choline chloride-urea appeared to maintain its structure, gradually undergoing mutual solubility only when slight interactions occurred between urea and surrounding water molecules. Rico et al. [41] proposed an extraction method based on sodium acetate-urea DES for bioactive compounds from melon peel, aiming for a more environmentally friendly approach. The study demonstrated that this DES exhibited remarkable environmental friendliness and cost-effectiveness, confirming the potential feasibility of using acetate salts as hydrogen bond acceptors in DES preparation.

It is worth noting that, compared to organic salts such as choline chloride, metal salts like sodium acetate (hereinafter referred to as acetates), as inorganic salts, exhibit higher thermal and chemical stability. Even when decomposed at high temperatures, the decomposition products are primarily harmless carbonates. Moreover, acetate salts demonstrate good miscibility and tunability with EG. However, most current research on DESs has focused on their fundamental thermophysical properties, with relatively little exploration of their thermal stability under medium-to-high temperature conditions and their synergistic effects with nanomaterials. In light of this, the present study selects ethylene glycol and acetate salts as base components to develop a series of DESs with enhanced thermal stability and a broader operating temperature range. Additionally, by doping with carbon nanotubes (CNTs), the heat transfer performance of these DESs is further improved. This research aims to provide new insights and technical support for the development of novel heat transfer fluids.

## 2. Materials and Methods

### *2.1. Materials*

Anhydrous sodium acetate (SA, $CH_3COONa$, analytical grade), anhydrous potassium acetate (PA, $CH_3COOK$, analytical grade), and anhydrous calcium acetate (CA, $Ca(CH_3COO)_2$, analytical grade) were purchased from Shanghai Aladdin Biochemical Technology Co., Ltd., Shanghai, China. Ethylene glycol (EG, $HOCH_2CH_2OH$, analytical grade) was obtained from Shanghai Macklin Biochemical Technology Co., Ltd., Shanghai, China Multi-walled carbon nanotubes (50 nm) were supplied by Nanjing Xianfeng Nanomaterials Technology Co., Ltd., Nanjing, China.

### *2.2. Preparation*

The ethylene glycol-acetate DESs were prepared using the melt blending method. Precise amounts of EG and sodium acetate (SA) with molar ratios of 4:1, 5:1, and 6:1, EG and potassium acetate (PA) with molar ratios of 4:1, 5:1, and 6:1, EG and calcium acetate (CA) with molar ratios of 24:1, 30:1, and 36:1 were weighed using an analytical balance. A total of 120 g was weighed per batch, with a weighing error of less than ±0.0025%. The components were then mixed in a 200 mL flask and heated under stirring at 80 °C and 300 rpm for 1 h until the solvent became clear and transparent, and no solid salt particles of the acetate were observed (Figure 1). The mixture was then cooled to room temperature to form a stable homogeneous system, resulting in ethylene glycol -acetate DESs at different molar ratios. The specific compositions and naming of the samples are listed in Table 1. Since ethylene glycol has poor miscibility with calcium acetate, larger molar ratios were selected for this mixture.

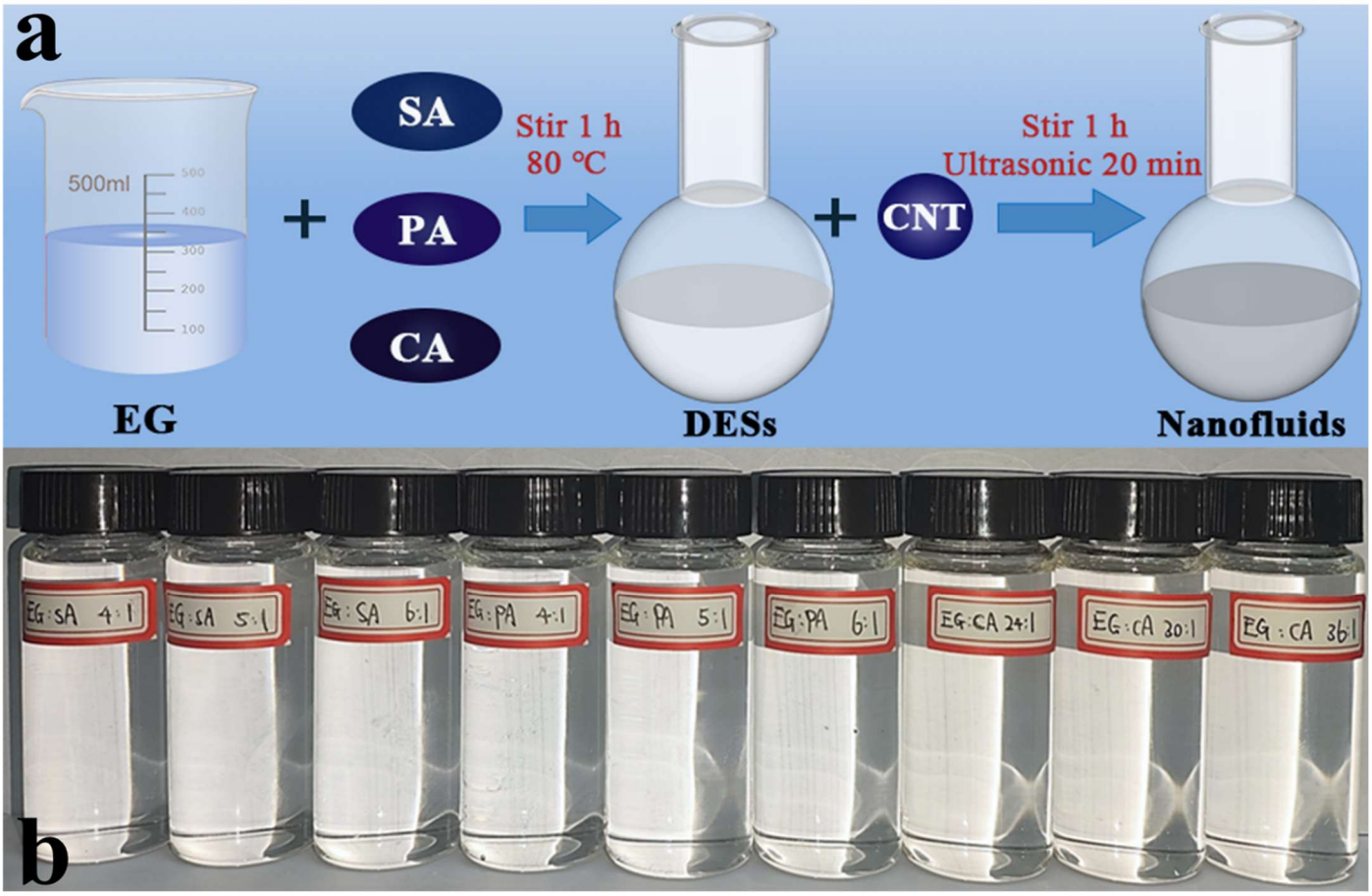


**Figure 1.** (**a**) Ethylene glycol-acetate DESs and nanofluid preparation process diagram; (**b**) the prepared ethylene glycol-acetate DESs.

**Table 1.** Scale strategy of ethylene glycol-acetate DESs.

| Sample | Ethylene Glycol (g) | Sodium Acetate (g) | Potassium Acetate (g) | Calcium Acetate (g) |
|---|---|---|---|---|
| EG:SA-4:1 | 90.199 | 29.801 | 0 | 0 |
| EG:SA-5:1 | 94.913 | 25.087 | 0 | 0 |
| EG:SA-6:1 | 98.340 | 21.660 | 0 | 0 |
| EG:PA-4:1 | 86.004 | 0 | 33.996 | 0 |
| EG:PA-5:1 | 91.170 | 0 | 28.830 | 0 |
| EG:PA-6:1 | 94.973 | 0 | 25.027 | 0 |
| EG:CA-24:1 | 108.482 | 0 | 0 | 11.518 |
| EG:CA-30:1 | 110.605 | 0 | 0 | 9.395 |
| EG:CA-36:1 | 112.067 | 0 | 0 | 7.933 |

The DES-based nanofluids were prepared using the “two-step method”, with the optimized DES composition as the base fluid and CNTs as the nanoparticles. After preparing the base DES, the nanoparticles were mixed with the solution at a specified mass ratio and sealed in a centrifuge tube. The mixture was then placed in a KQ5200DE ultrasonic

cleaner (Kunshan Ultrasonic Instrument Co., Ltd., Suzhou, China) for ultrasonic treatment, ensuring thorough dispersion of the nanoparticles and resulting in the formation of a stable nanofluid. The dispersion stability of the nanofluids was investigated by exploring the effects of different nanoparticle concentrations, base fluid pH values, and ultrasonic treatment times.

### *2.3. Characterization*

Thermal stability analysis of the samples was conducted using a thermogravimetric analyzer (Shanghai Jingke Tianmei RZY-1). A 20 mg sample was weighed using an analytical balance and heated from room temperature to 350 °C at a rate of 10 °C/min under a nitrogen atmosphere as the protective gas. The mass loss rate and mass loss kinetics at different temperatures were obtained by software analysis.

The boiling points of the DESs were determined using a heating device and thermocouple. A suitable amount of the sample was rinsed into a test tube, and approximately 5 mL of the sample was added. Clean glass beads were added to prevent bumping. The thermocouple was fixed to the side of the test tube, ensuring that the probe tip was above the liquid level of the sample. A data logger was used to record the temperature changes, and an alcohol lamp was ignited to provide continuous heating. Heating was continued until the temperature stabilized, at which point the temperature was recorded as the boiling point of the sample. Multiple measurements were taken, and the average value was used.

The melting point of the sample was measured using an ethanol-drikold bath and an alcohol thermometer. A suitable amount of the sample was rinsed into a test tube, and approximately 10 mL of the sample was added. The test tube was then immersed in a beaker containing ethanol and fixed using a test tube clamp and iron stand. A small amount of drikold was added to the beaker to ensure that it did not directly contact the test tube. After the drikold was completely sublimated, more were added. A thermometer was inserted into the test tube, and the sample was stirred up and down. Once the sample cooled and formed a gel-like mass, the temperature was recorded as the freezing point. Multiple measurements were taken, and the average value was used.

The specific heat capacity of EG and each DES was measured using a differential scanning calorimeter (DSC 25, TA Instruments, New Castle, DE, USA) with the sapphire method. Three separate tests were conducted: a blank crucible test, a sapphire standard sample test, and a sample test. The temperature range was set from 0 to 90 °C with a heating rate of 10 °C/min. When calculating the specific heat capacity of the sample, the data from the blank crucible test were subtracted. The specific heat capacity of the sample was calculated using the following formula:

$$c_2 = \frac{(Y_2 - Y_0)m_1}{(Y_1 - Y_0)m_2} c_1 \quad (1)$$

where $Y_2$, $Y_1$, and $Y_0$ represent the heat flow values measured by DSC for the sample, standard sapphire, and blank crucible at different temperatures, respectively; $m_2$ and $m_1$ are the masses of the sample and standard sapphire; $c_2$ and $c_1$ are the specific heat capacities of the sample and standard sapphire, with the specific heat capacity of the standard sapphire being known [42].

The thermal conductivity of the samples was measured using a 9P3001-16003 device (Xi'an Xiaxi Electronic Technology Co., Ltd., Xi'an, China) employing the transient hot-wire method. A 50 mL jacketed beaker was rinsed with 5 mL of the sample, and approximately 40 mL of the sample was added. The thermal conductivity sensor, equipped with a temperature monitor, was completely immersed in the sample to be tested. The jacketed beaker was connected to a constant-temperature water bath, and the water pump of the bath was activated to control the sample temperature. Once the temperature sensor reached the desired testing temperature, thermal equilibrium was monitored to ensure the accuracy of the measurements. Five measurements were taken for each sample at each temperature point.

The dynamic viscosity of the samples was measured using a rotational viscometer (Shanghai Fangrui Instruments, Shanghai, China, LVDV-2T). The sample liquid was added to the cup until the rotor was submerged, and the temperature of the surrounding environment was adjusted by controlling the temperature of the constant-temperature bath. During the measurement, the synchronous motor rotated at a constant speed, and the rotor was subjected to the viscous torque of the fluid. The viscous resistance was proportional to the viscosity, and the instrument calculated the viscosity data. Five measurements were taken for each sample at each temperature point.

The density of the samples was measured using a buoyancy densitometer. A 200 mL jacketed graduated cylinder was rinsed with 10 mL of the sample, and approximately 180 mL of the sample was added. The jacketed graduated cylinder was connected to a constant-temperature water bath, and the water pump of the bath was activated to control

the sample temperature. Once the thermometer reached the required testing temperature, the density of the sample was read using the buoyancy densitometer.

The dispersion stability of the nanofluids was qualitatively observed using a sedimentation observation method. The photothermal conversion efficiency of the nanofluids was tested by constructing a photothermal conversion experimental platform, which consisted mainly of a simulated sunlight lamp, a temperature data logger, and the testing unit.

## 3. Results and Discussion

### *3.1. Thermal Stability of DESs*

The thermogravimetric (TG) and differential thermogravimetric (DTG) curves of the samples obtained from thermogravimetric analysis are shown in Figure 2. Selecting specific temperatures corresponding to certain percentages of mass loss is instrumental in assessing a material's thermal stability and decomposition behavior. Typically, temperatures at 5% and 30% mass loss are chosen as key indicators, representing the onset of decomposition and significant structural degradation, respectively. A 5% mass loss often signifies initial chemical bond breakage or the release of small molecules, marking a critical point in the material's thermal stability. At 30% mass loss, the material has typically undergone substantial decomposition, with its structure severely compromised and functional properties largely lost, rendering it unsuitable for its intended applications [43]. A comparison of the TGA curve with the original EG revealed that the initial decomposition temperatures of the DESs shifted to higher temperatures. Among these, the EG-PA DESs exhibited a consistent shift, with the initial decomposition temperature increasing by 40–50 °C and the temperature for complete structural degradation rising by 35–45 °C. For the EG-CA DESs, the increase was smaller, with the temperature for complete structural degradation rising by 10–20 °C. From the DTG curves, it can be seen that the maximum decomposition rate of EG-SA DESs and EG-PA DESs shifted to higher temperatures and decreased, while the maximum decomposition rate of EG-CA DESs occurred at a temperature close to that of EG, with a slightly higher decomposition rate. Overall, the addition of acetate salts altered the original hydrogen bond network of EG, enhancing the intermolecular forces and improving thermal stability. However, the improvement was influenced by the type and blending amount of acetate salt; after the addition of potassium acetate, the enhancement in thermal stability was particularly notable. In contrast, CA, with its relatively poor inherent stability, contributed only limited improvement to the thermal stability of EG-CA DESs. Furthermore, with the increase in the acetate salt blending ratio, an overall improvement in the thermal stability of the samples was observed.

It should be acknowledged that TGA-based thermal stability assessments may have certain limitations. Since TGA focuses primarily on mass changes over a given temperature range, factors such as heating rate, sample atmosphere, and potential side reactions can influence how thermal stability is interpreted. Moreover, TGA alone does not provide direct insight into morphological or structural changes that may affect the material's performance. Consequently, it is generally recommended to employ a higher-precision TGA or combine TGA with other testing methods to gain a more comprehensive understanding of a material's thermal behavior.

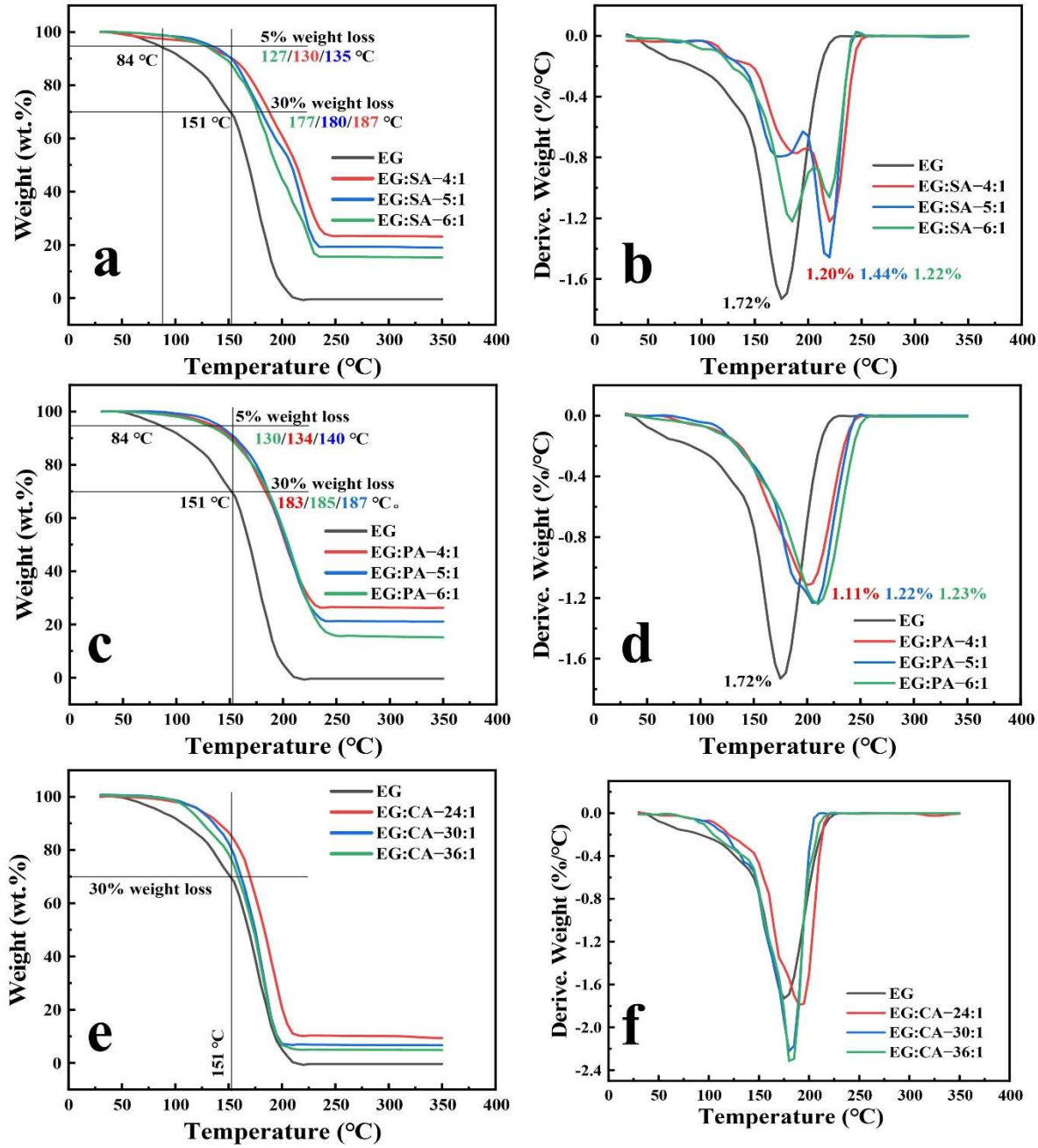


**Figure 2.** (**a**) TG curve illustrating mass-loss behavior of EG-SA DESs; (**b**) DTG curve highlighting decomposition steps of EG-SA DESs; (**c**) TG curve of EG-PA DESs; (**d**) DTG curve of EG-PA DESs; (**e**) TG curve of EG-CA DESs; (**f**) DTG curve of EG-CA DESs.

### *3.2. Liquid Phase Temperature Range of DESs*

The liquid phase temperature range of each sample obtained from testing is shown in Figure 3. As can be observed, due to the inherent properties of DES, the addition of acetate salts caused an increase in entropy, and in order to achieve a higher level of disorder (liquid state), the mixture underwent a phase transition at lower temperatures. The DES exhibited a general decrease in melting point, all of which were lower than the melting points of the original components, further confirming that the prepared solution was a DES [44]. Meanwhile, due to the formation of new hydrogen bonds, intermolecular interactions were strengthened, leading to a moderate increase in the boiling points of EG-SA DESs and EG-PA DESs. However, the relatively poor stability of CA caused the DES to experience premature boiling. Overall, the addition of SA and PA effectively broadened the liquid phase temperature range of EG, extending its application as a heat transfer fluid and allowing it to demonstrate higher adaptability and flexibility in various industrial heat transfer processes.

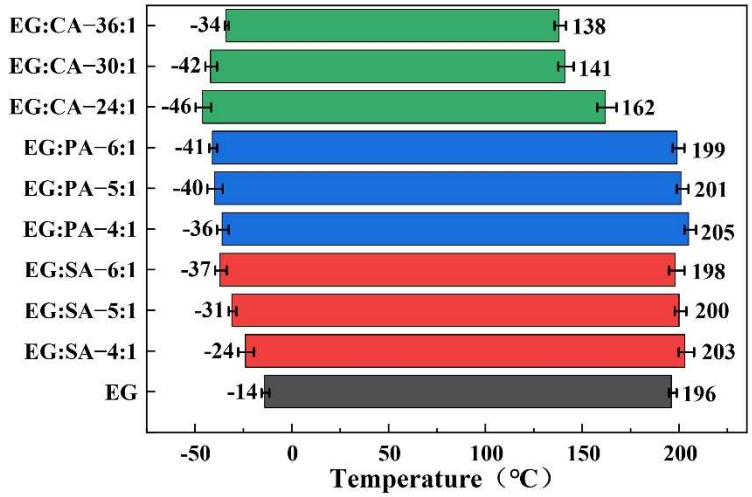


**Figure 3.** Liquid phase temperature range of ethylene glycol and ethylene glycol-acetate DESs.

### *3.3. Rheological and Thermal Properties of DESs*

Figure 4a–c show the viscosity variation curves of EG-SA DESs, EG-PA DESs, and EG-CA DESs from 25 °C to 60 °C. As the acetate salt component increased, the viscosity of the DESs exhibited an increasing trend, with EG-PA DESs showing the smallest increase in viscosity. Additionally, as the temperature increased, molecular motion intensified, causing the viscosity of all samples to decrease gradually. Figure 4d–f show the thermal conductivity variation curves of EG-SA DESs, EG-PA DESs, and EG-CA DESs from 25 °C to 65 °C. Due to the larger proportion of salt components in EG-SA DESs and EG-PA DESs, the intermolecular arrangement became more complex, which hindered the original heat transfer network, resulting in a decrease in both thermal conductivity and specific heat capacity. In contrast, EG-CA DESs, with a smaller salt component, slightly reinforced the original heat transfer network, leading to a slight increase in thermal conductivity. Figure 4g–i show the specific heat capacity variation curves of the DESs from 25 °C to 85 °C. The trends and influencing factors were similar to those for thermal conductivity. The enhanced intermolecular interactions in deep eutectic solvents increased resistance during energy transfer, meaning more energy was required to induce molecular vibration or movement, leading to a decrease in specific heat capacity. However, the addition of CA increased intermolecular activity, leading to a slight rise in specific heat capacity. Furthermore, as the temperature increased, molecular motion intensified, and the thermal conductivity and specific heat capacity of all samples showed an upward trend. Figure 4j–l show the density variation curves of the DESs from 25 °C to 65 °C. Density was primarily influenced by the density of the original components, with PA having a higher density, resulting in a higher density of the corresponding DES. As the temperature increased, molecular motion intensified and molecular distance increased, causing the volume of all samples to expand and the density to decrease.

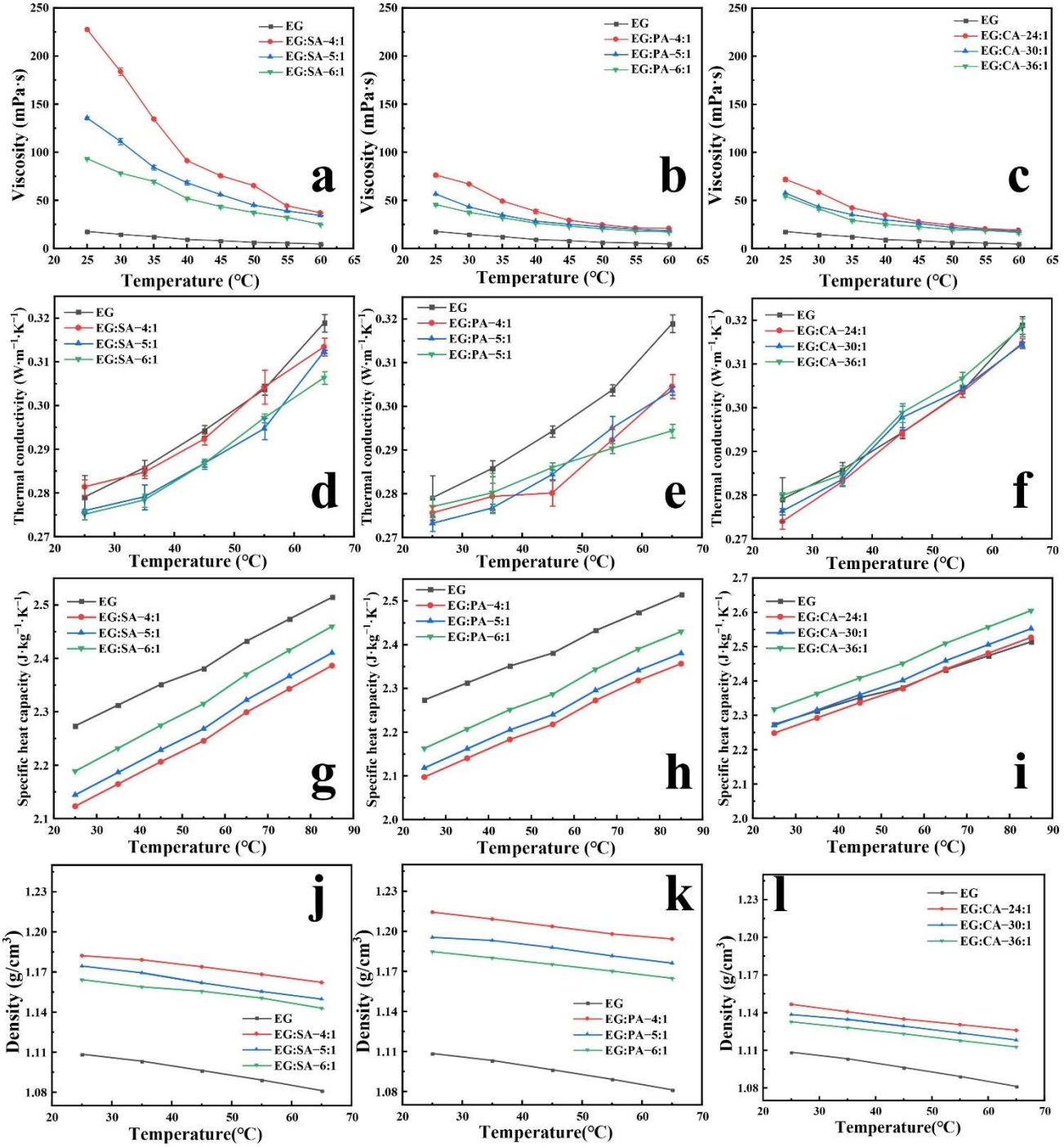


**Figure 4.** (**a**) Viscosity of EG-SA DESs at 25–60 °C; (**b**) viscosity of EG-PA DESs at 25–60 °C; (**c**) viscosity of EG-CA DESs at 25–60 °C; (**d**) thermal conductivity of EG-SA DESs at 25–65 °C; (**e**) thermal conductivity of EG-PA DESs at 25–65 °C; (**f**) thermal conductivity of EG-CA DESs at 25–65 °C; (**g**) specific heat capacity of EG-SA DESs at 25–85 °C; (**h**) specific heat capacity of EG-PA DESs at 25–85 °C; (**i**) specific heat capacity of EG-CA DES at 25–85 °Cs; (**j**) density of EG-SA DESs at 25–65 °C; (**k**) density of EG-PA DESs at 25–65 °C; (**l**) density of EG-CA DESs at 25–65 °C.

### *3.4. Dispersion Stability of DES Based Nanofluids*

EG:PA-5:1 was selected as the base fluid for the nanofluid due to its excellent thermal stability, relatively broad liquid range, low viscosity, moderate density, and minimal decrease in thermal conductivity and specific heat capacity. The dispersion stability of the nanofluid was qualitatively studied through sedimentation observation, focusing on the effects of nanoparticle concentration, ultrasonic mixing time, and base fluid pH value. Insufficient ultrasonic mixing time leads to poor dispersion of the nanoparticles, causing agglomeration and resulting in suboptimal dispersion. Excessive ultrasonic mixing time can cause intense collisions between nanoparticles, leading to agglomeration or even surface chemical changes, which also negatively impact dispersion. When the pH value of the base fluid is close to the

isoelectric point of the nanoparticles, the surface charge decreases, reducing electrostatic repulsion between particles, which promotes agglomeration. When the pH value is far from the isoelectric point, the nanoparticles carry a higher positive or negative charge, increasing electrostatic repulsion and enhancing dispersion stability.

As shown in Figure 5a, the dispersion stability of nanofluids with carbon nanotube concentrations of 0.06 wt.%, 0.08 wt.%, and 0.12 wt.% was explored under the conditions of an unadjusted base fluid pH and ultrasonic mixing for 20 min. After 12 h of standing, the 0.12 wt.% sample exhibited significant agglomeration and sedimentation, the 0.08 wt.% sample showed slight sedimentation and the 0.06 wt.% sample showed almost no sedimentation. As shown in Figure 5b, under the conditions of an unadjusted base fluid pH and a nanoparticle concentration of 0.06 wt.%, the effect of different ultrasonic mixing times (60 min, 40 min, and 20 min) on the dispersion stability of the nanofluid was investigated. After 12 h of standing, the sample subjected to 60 min of ultrasonic mixing showed severe agglomeration and sedimentation, the 40-min sample exhibited noticeable agglomeration and sedimentation, and the 20-min sample showed almost no sedimentation. The pH of the DES base fluid was measured to be approximately 9. After adding acetic acid as a buffering agent, the pH of the base fluid was adjusted to 8 and 7. As shown in Figure 5c, the effect of different base fluid pH values on the dispersion stability of nanofluids with 0.08 wt.% nanoparticle concentration and 20 min of ultrasonic mixing was explored. After 12 h of standing, the sample with pH 7 showed noticeable agglomeration and sedimentation, the sample with pH 8 showed almost no sedimentation, and the sample with pH 9 showed slight sedimentation. After 24 h of standing, the sample with pH 7 showed severe agglomeration and sedimentation, the sample with pH 8 showed almost no sedimentation, and the sample with pH 9 showed some degree of agglomeration and sedimentation. After 36 h of standing, the sample with pH 8 showed some degree of agglomeration and sedimentation, and the sample with pH 9 showed significant agglomeration and sedimentation. In summary, smaller nanoparticle concentrations, shorter ultrasonic mixing times, and a pH of 8 were more effective in maintaining the dispersion stability of carbon nanotubes in EG-PA DESs.

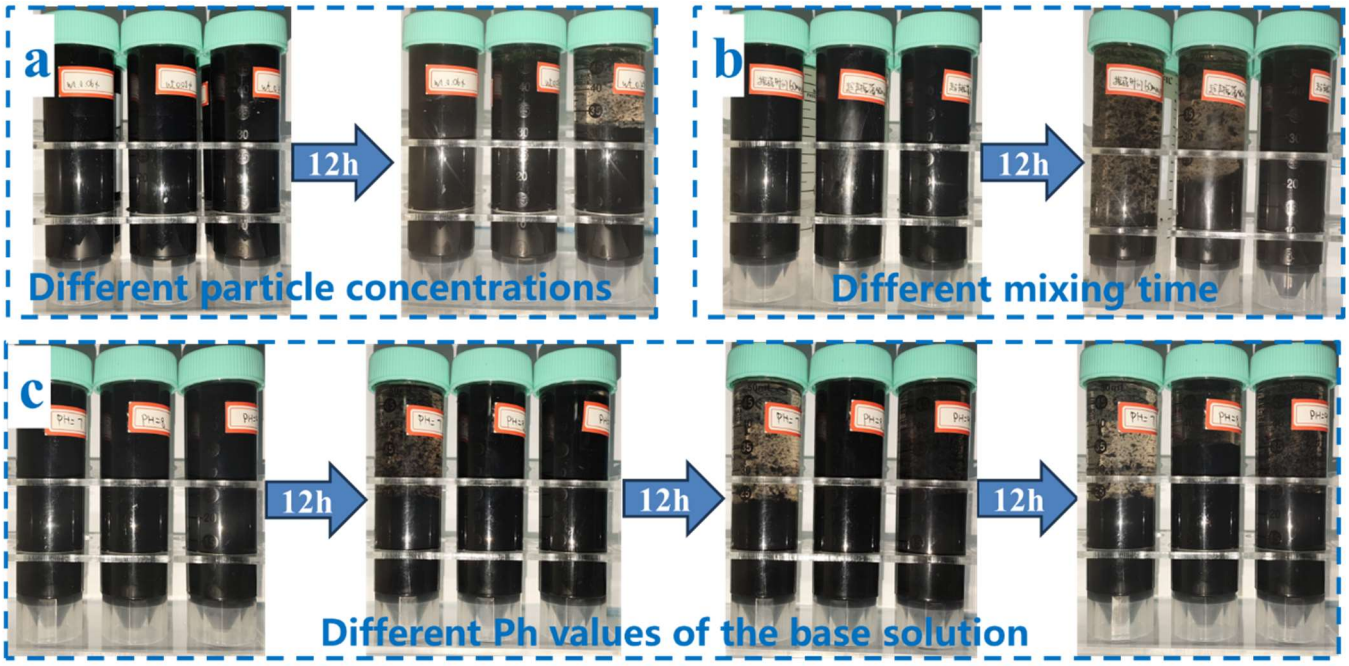


**Figure 5.** (**a**) Effect of different nanoparticle concentrations on dispersion stability; (**b**) effect of different ultrasonic mixing times on dispersion stability; (**c**) effect of different base fluid pH values on dispersion stability.

### *3.5. Thermal Stability and Thermal Properties of DES Based Nanofluids*

As shown in Figure 6a,b, after adding 0.08 wt.% nanoparticles to the DES base fluid to prepare the nanofluid, the maximum decomposition rate further decreased and shifted to higher temperatures. This resulted in a delay in the overall thermal degradation process and an improvement in thermal stability. This effect can be attributed to the interaction between the nanoparticles and the base fluid, which forms a protective effect. Additionally, the high surface area of the nanoparticles allows them to disperse heat and reduce the activation of molecular motion effectively. As shown in Figure 6d, compared to the DES base fluid, the specific heat capacity of the nanofluid increased by approximately 7.5%. This is because carbon nanotubes possess a very high surface area, and when added to the fluid, they increase the

available surface area for heat exchange. This change enhances the fluid's energy absorption and improves heat distribution, effectively increasing the overall heat storage capacity of the fluid thereby raising the total heat capacity of the nanofluid. Additionally, as shown in Figure 6e, after the incorporation of nanoparticles into the base fluid, thermal conductivity increased by approximately 3~4%. This improvement is due to the heat conduction bridging effect between nanoparticles, which enhances heat transfer efficiency within the base fluid. Moreover, the nanoparticles increase the contact area for heat transfer, alter the structure of the thermal boundary layer, and enhance both conduction and convection, thus improving the overall thermal conductivity of the base fluid. As predicted, the incorporation of nanoparticles also led to a slight increase in the fluid density.

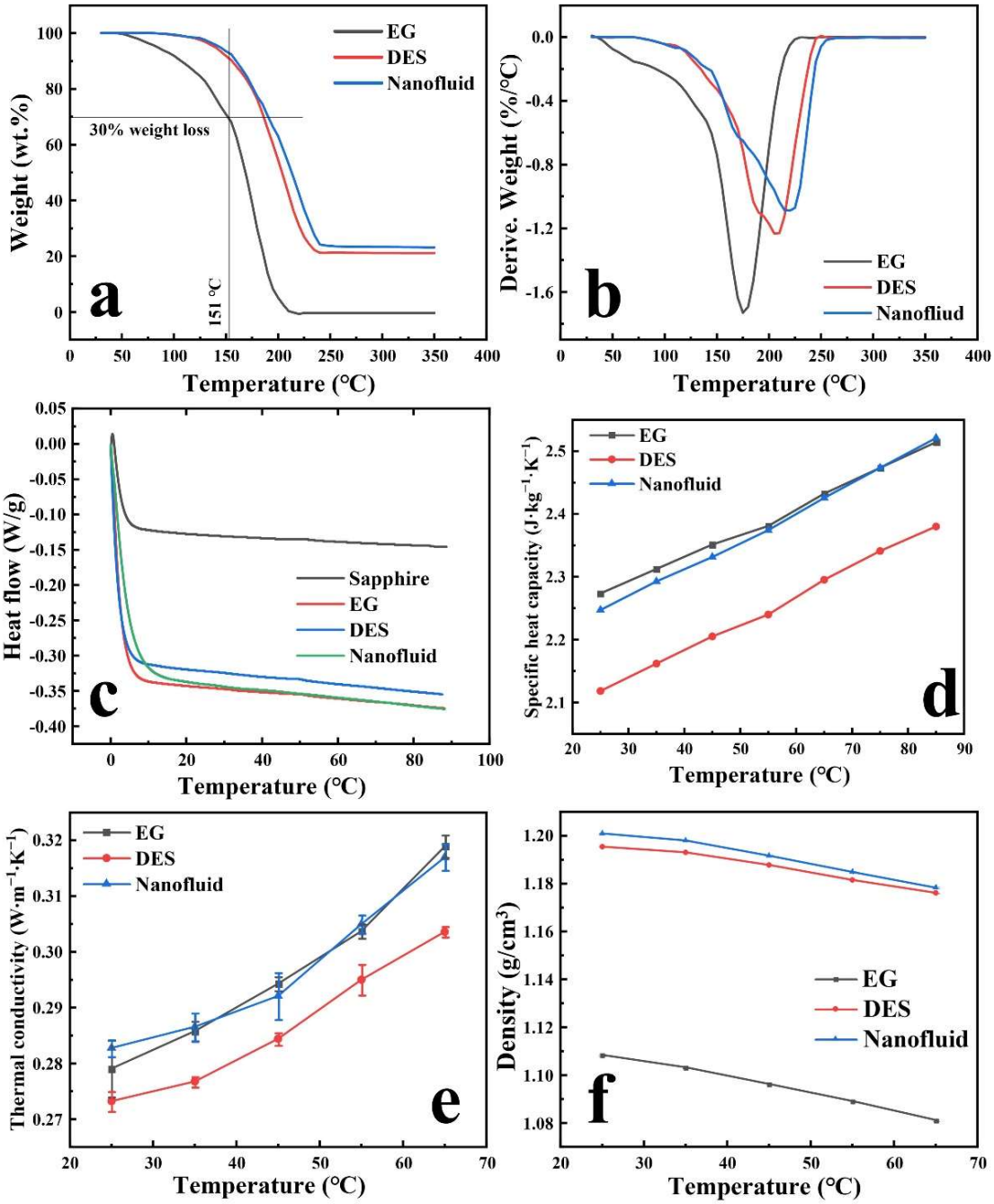


**Figure 6.** (**a**) TG curve of the nanofluid; (**b**) DTG curve of the nanofluid; (**c**) heat flow curve for specific heat capacity measurement of the nanofluid using the sapphire method; (**d**) specific heat capacity of the nanofluid; (**e**) thermal conductivity of the nanofluid; (**f**) density of the nanofluid.

### *3.6. Photothermal Conversion Efficiency of DES Based Nanofluids*

The photothermal conversion experimental platform constructed is shown in Figure 7a. The test unit consists of a 50 mL beaker containing 50 mL of the sample, with temperature measurement points placed at the 5 mL, 25 mL, and 45 mL marks, representing the bottom, middle, and top layers of the fluid, respectively. The outside of the beaker is wrapped with wool for thermal insulation. Direct irradiation is provided by a solar simulator, with the radiation intensity of the simulated light source measured by a light power density meter at 1500 W/m$^2$. Figure 7b–d show the photothermal conversion curves obtained from the tests. The photothermal conversion efficiency of each fluid was calculated using the following formula:

$$\eta = \frac{Q_f}{Q} = \frac{c_f m_f}{IA} \cdot \frac{\Delta T}{\Delta t} \quad (2)$$

In the equation, $Q_f$ represents the heat absorbed by the fluid under illumination, $Q$ represents the heat from the light source irradiated on the medium, $c_f$ represents the specific heat capacity of the nanofluid, mf represents the mass of the fluid, $\Delta T$ represents the temperature change of the fluid, $\Delta t$ represents the duration of the illumination heating, $I$ represents the light intensity, and $A$ represents the area of the fluid exposed to the light [45].

As shown in Figure 7e–g, during the T1 period (illumination time from 0 to 1000 s), the photothermal conversion efficiency of the upper layer nanofluid reached 42.7%, exceeding those of DES and EG by 43.3% and 52.5%, respectively. The pronounced enhancement in the CNT-based nanofluid's photothermal conversion efficiency can be primarily attributed to the outstanding properties of CNTs. Owing to their extensive conjugated π-electron network, CNTs can absorb light across a broad spectral range, thereby converting incident photons into thermal energy with high efficiency. Furthermore, their large aspect ratio and exceptional thermal conductivity facilitate rapid heat transfer and distribution throughout the fluid. As a result, these synergistic characteristics collectively yield significantly higher photothermal conversion efficiencies compared to DES and EG. The photothermal conversion efficiencies of the nanofluid in the middle and lower layers during the T1 and T2 periods (illumination time from 2000 to 3000 s) were also higher than those of DES and EG. However, due to the relatively low light transmittance of the nanofluid in the lower layer, the temperature approached equilibrium after the T3 period (illumination time from 4000 to 5000 s), resulting in a lower photothermal conversion efficiency. Overall, during the heating phase at 60 °C and for fluid layers within 30 mm, the photothermal conversion efficiency of the CNT-based nanofluid was significantly superior to that of DES and EG.

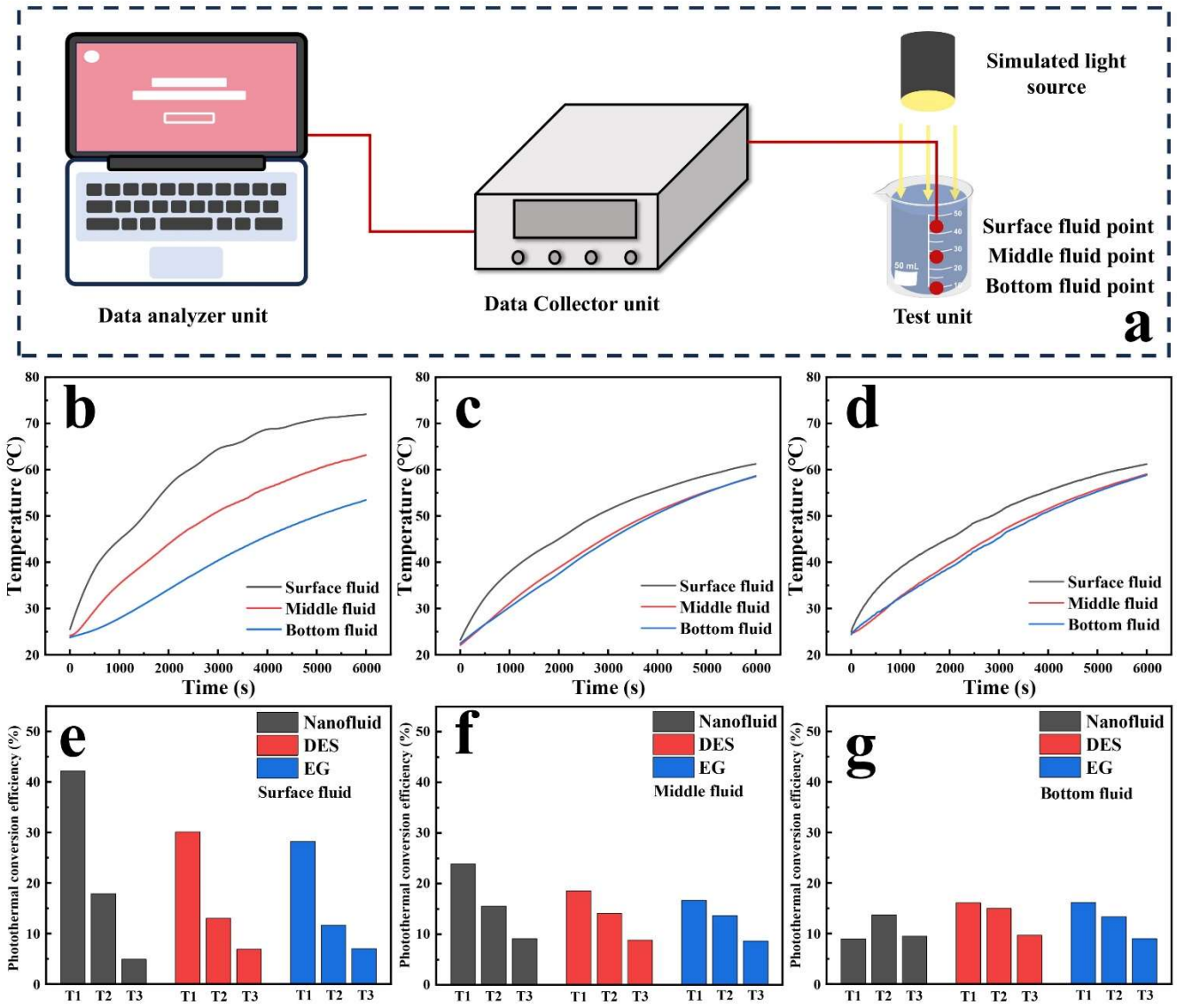


**Figure 7.** (**a**) Schematic diagram of photothermal conversion experimental platform; (**b**) photothermal conversion curve of the nanofluid; (**c**) photothermal conversion curve of the DES; (**d**) photothermal conversion curve of EG; (**e**) photothermal conversion efficiency of the upper layer fluid at different time intervals (T1: 0–1000 s, T2: 2000–3000 s, T3: 4000–5000 s); (**f**) photothermal conversion efficiency of the middle layer fluid at different time intervals; (**g**) photothermal conversion efficiency of the bottom layer fluid at different time intervals.

## 4. Conclusions

This study, through systematic experiments and analysis, developed a series of DESs based on ethylene glycol and different types of acetates and conducted an in-depth investigation of their thermophysical properties. The results showed that the DES formed from the combination of EG and PA exhibited excellent thermal stability, with its liquid phase temperature range expanded from −14~196 °C to −40~201 °C, significantly enhancing its adaptability as a heat transfer fluid. Building on this, EG:PA-5:1 DES was selected as the base fluid, and nanofluids were prepared by doping with 0.08 wt.% carbon nanotubes. The dispersion stability and thermal performance were further improved by optimizing ultrasonic mixing time and base fluid pH. Experimental data indicated that the introduction of carbon nanotubes significantly enhanced the heat transfer properties of the nanofluid, with thermal conductivity increasing by approximately 3%, specific heat capacity rising by 7.5%, and photothermal conversion efficiency reaching 42.7% during the heating phase below 60 °C. This confirmed the excellent synergistic effect between the nanoparticles and DES, and demonstrated the potential applications of this system in efficient energy management.

**Acknowledgments**

The authors express gratitude to the Fundamental Research Funds for the Central Universities (NO. 2023ZDPY12) and Natural Science Foundation of Hubei Province (No. 2023AFB428). We also gratefully acknowledge Hua Wei and Rui Zhou from the Advanced Analysis & Computation Center at CUMT for their valuable assistance with chemical analysis.

**Author Contributions**

Conceptualization, C.L. and X.Z.; Methodology, C.L.; Software, H.G.; Validation, X.D., P.L. and J.H.; Formal Analysis, X.Z. and X.D.; Investigation, J.Z.; Resources, C.L.; Data Curation, G.L.; Writing—Original Draft Preparation, X.Z.; Writing—Review & Editing, C.L.; Visualization, X.D.; Supervision, J.Z.; Project Administration, W.H.; Funding Acquisition, C.L.

**Ethics Statement**

Not applicable.

**Informed Consent Statement**

Not applicable.

**Data Availability Statement**

The data that support the findings of this study are available from the corresponding author upon reasonable request.

**Funding**

This work was supported by the Fundamental Research Funds for the Central Universities (NO. 2023ZDPY12) and Natural Science Foundation of Hubei Province (No. 2023AFB428).

**Declaration of Competing Interest**

The authors declare that they have no known competing financial interests or personal relationships that could have appeared to influence the work reported in this paper.

**References**

1. Zhang H, Wang L, Xi S, Xie H, Yu W. 3D porous copper foam-based shape-stabilized composite phase change materials for high photothermal conversion, thermal conductivity and storage. *Renew. Energy* **2021**, *175*, 307–317. doi:10.1016/j.renene.2021.05.019.
2. Vidal F, van der Marel ER, Kerr RWF, McElroy C, Schroeder N, Mitchell C, et al. Designing a circular carbon and plastics economy for a sustainable future. *Nature* **2024**, *626*, 45–57. doi:10.1038/s41586-023-06939-z.
3. Song M, Shao F, Wang L, Xie H, Yu W. Biomass-derived porous carbon aerogels for effective solar thermal energy storage and atmospheric water harvesting. *Sol. Energy Mater. Sol. Cells* **2023**, *262*, 112532. doi:10.1016/j.solmat.2023.112532.
4. Subramaniam Y, Loganathan N, Subramaniam T, Bulut U. The impact of energy security on environmental degradation: New evidence from developing countries. *Environ. Sci. Pollut. Res.* **2023**, *30*, 108802–108824. doi:10.1007/s11356-023-29965-w.
5. Cui Y, Liu D, Shu Y. Study on Heat Transfer Characteristics of Graphene Nanofluids in Mini-Channels of Thermal Integrated Building. *Entropy* **2023**, *25*, 712. doi:10.3390/e25050712.
6. Albà CG, Alkhatib III, Llovell F, Vega LF. A novel approach for designing efficient and sustainable cooling cycles with low global warming potential refrigerants. *Appl. Therm. Eng.* **2024**, *246*, 122895. doi:10.1016/j.applthermaleng.2024.122895.
7. Shao F, Wang L, Luo R, Yu W, Xie H. Shape-Stable Hybrid Emulsion Gel with Sodium Acetate Trihydrate and Paraffin Wax for Efficient Solar Energy Storage and Building Thermal Management. *ACS Appl. Mater. Interfaces* **2023**, *15*, 38474–38484. doi:10.1021/acsami.3c07429.
8. Mahian O, Bellos E, Markides CN, Taylor RA, Alagumalai A, Yang L, et al. Recent advances in using nanofluids in renewable energy systems and the environmental implications of their uptake. *Nano Energy* **2021**, *86*, 106069. doi:10.1016/j.nanoen.2021.106069.
9. Ma Y, Yang Y, Li T, Hussain S, Zhu M. Deep eutectic solvents as an emerging green platform for the synthesis of functional materials. *Green Chem.* **2024**, *26*, 3627–3669. doi:10.1039/D3GC04289H.
10. Li Z, Li Q. Ultrasonic-Assisted Efficient Extraction of Coumarins from Peucedanum decursivum (Miq.) Maxim Using Deep Eutectic Solvents Combined with an Enzyme Pretreatment. *Molecules* **2022**, *27*, 5715. doi:10.3390/molecules27175715.

11. González-Campos JB, Pérez-Nava A, Valle-Sánchez M, Delgado-Rangel LH. Deep eutectic solvents applications aligned to 2030 United Nations Agenda for Sustainable Development. *Chem. Eng. Process. -Process Intensif.* **2024**, *199*, 109751. doi:10.1016/j.cep.2024.109751.
12. Yu Y, Li S, Lu J, Xi F, Chen X, Wu D, et al. Green recycling of end-of-life photovoltaic modules via Deep-Eutectic solvents. *Chem. Eng. J.* **2024**, *499*, 155933. doi:10.1016/j.cej.2024.155933.
13. Song M, Cheng T, Li Y, Huang D, Huang X, Xie H, et al. Spongy hygroscopic hydrogels for efficient atmospheric water harvesting over a wide humidity range. *J. Clean. Prod.* **2024**, *461*, 142661. doi:10.1016/j.jclepro.2024.142661.
14. Álvarez MS, Longo MA, Rodríguez A, Deive FJ. The role of deep eutectic solvents in catalysis. A vision on their contribution to homogeneous, heterogeneous and electrocatalytic processes. *J. Ind. Eng. Chem.* **2024**, *132*, 36–49. doi:10.1016/j.jiec.2023.11.030.
15. Fan C, Liu Y, Sebbah T, Cao X. A Theoretical Study on Terpene-Based Natural Deep Eutectic Solvent: Relationship between Viscosity and Hydrogen-Bonding Interactions. *Glob. Chall.* **2021**, *5*, 2000103. doi:10.1002/gch2.202000103.
16. Banjare RK, Banjare MK, Behera K, Pandey S, Ghosh KK. Micellization Behavior of Conventional Cationic Surfactants within Glycerol-Based Deep Eutectic Solvent. *ACS Omega* **2020**, *5*, 19350–19362. doi:10.1021/acsomega.0c00866.
17. Chen Y, Yu D, Lu Y, Li G, Fu L, Mu T. Volatility of Deep Eutectic Solvent Choline Chloride:N-Methylacetamide at Ambient Temperature and Pressure. *Ind. Eng. Chem. Res.* **2019**, *58*, 7308–7317. doi:10.1021/acs.iecr.8b04723.
18. Bhattacharjee S, Dikki R, Gurkan B, Getman RB. Effect of water on eutectic solvents: Structural properties and physical interactions with $CO_2$. *J. Mol. Liq.* **2024**, *410*, 125569. doi:10.1016/j.molliq.2024.125569.
19. Emanuele E, Li Bassi A, Macrelli A, Mele C, Strada J, Bozzini B. Zinc Electrode Cycling in Deep Eutectic Solvent Electrolytes: An Electrochemical Study. *Molecules* **2023**, *28*, 957. doi:10.3390/molecules28030957.
20. Lim E, Yon Pang J-S, Lau EV. A comparative study of thermophysical properties between choline chloride-based deep eutectic solvents and imidazolium-based ionic liquids. *J. Mol. Liq.* **2024**, *395*, 123895. doi:10.1016/j.molliq.2023.123895.
21. Halder AK, Haghbakhsh R, Voroshylova IV, Duarte ARC, Cordeiro NDSM. Density of Deep Eutectic Solvents: The Path Forward Cheminformatics-Driven Reliable Predictions for Mixtures. *Molecules* **2021**, *26*, 5779. doi:10.3390/molecules26195779.
22. Shi D, Zhou F, Mu W, Ling C, Mu T, Yu G, et al. Deep insights into the viscosity of deep eutectic solvents by an XGBoost-based model plus SHapley Additive exPlanation. *Phys. Chem. Chem. Phys.* **2022**, *24*, 26029–26036. doi:10.1039/D2CP03423A.
23. Sun W, Liu Q, Zhao J, Muhammad Ali H, Said Z, Liu C. Experimental study on sodium acetate trihydrate/glycerol deep eutectic solvent nanofluids for thermal energy storage. *J. Mol. Liq.* **2023**, *372*, 121164. doi:10.1016/j.molliq.2022.121164.
24. Dehury P, Chaudhari S, Banerjee T, Kumar Das S. Prediction of thermophysical properties of deep eutectic solvent-based organic nanofluids: A machine learning approach. *J. Mol. Liq.* **2024**, *411*, 125809. doi:10.1016/j.molliq.2024.125809.
25. Quitian-Ardila LH, Garcia-Blanco YJ, Daza-Barranco LM, Schimicoscki RS, Andrade DEV, Franco AT. Improving the rheological and thermal stability of water-based drilling fluids by incrementing xanthan gum concentration. *Phy. Fluids* **2024**, *36*, 14. doi:10.1063/5.0230214.
26. Doninelli M, Di Marcoberardino G, Iora P, Gelfi M, Invernizzi CM, Manzolini G. Silicon Tetrachloride as innovative working fluid for high temperature Rankine cycles: Thermal Stability, material compatibility, and energy analysis. *Appl. Therm. Eng.* **2024**, *249*, 123239. doi:10.1016/j.applthermaleng.2024.123239.
27. Liu S, Yu D, Chen Y, Shi R, Zhou F, Mu T. High-Resolution Thermogravimetric Analysis Is Required for Evaluating the Thermal Stability of Deep Eutectic Solvents. *Ind. Eng. Chem. Res.* **2022**, *61*, 14347–14354. doi:10.1021/acs.iecr.2c02240.
28. Chen Y, Yang Z, Hu Y, Zhang Y, He H. Thermal stability of trifluoroiodomethane (R13I1) as an environmentally friendly working fluid for refrigeration and heat pump systems: Investigations and improvement strategies. *Appl. Therm. Eng.* **2024**, *248*, 123159. doi:10.1016/j.applthermaleng.2024.123159.
29. Pei X, Tian H, Zheng Z, Wang Y, Hou L. Secondary Flow Effect on Supercritical Kerosene Oxidation Deposition and Heat Transfer in a Coiled Tube. *ACS Omega* **2022**, *7*, 23978–23987. doi:10.1021/acsomega.2c02848.
30. Kwasi-Effah CC, Egware HO, Obanor AI, Ighodaro OO. Development and characterization of a quaternary nitrate based molten salt heat transfer fluid for concentrated solar power plant. *Heliyon* **2023**, *9*, e16096. doi:10.1016/j.heliyon.2023.e16096.
31. Borode A, Tshephe T, Olubambi P, Sharifpur M, Meyer J. Stability and Thermophysical Properties of GNP-$Fe_2O_3$ Hybrid Nanofluid: Effect of Volume Fraction and Temperature. *Nanomaterials* **2023**, *13*, 1238. doi:10.3390/nano13071238.
32. Vigneshwaran P, Shaik S, Suresh S, Abbas M, Saleel CA, Cuce E. Solar Salt with CNTs as a Potential Phase Change Material for High-Temperature Applications: Investigations on Thermal Properties and Chemical Stability. *ACS Omega* **2023**, *8*, 17563–17572. doi:10.1021/acsomega.2c07571.
33. Al-Kayiem HH, Oladosu TL, Gilani SIU, Baheta AT. Molecular dynamics of binary deep eutectic solvents as biocompatible working fluids in heat and mass transfer systems. *J. Mol. Liq.* **2021**, *342*, 117493. doi:10.1016/j.molliq.2021.117493.
34. Majid MF, Mohd Zaid HF, Kait CF, Ghani NA, Jumbri K. Mixtures of tetrabutylammonium chloride salt with different glycol structures: Thermal stability and functional groups characterizations. *J. Mol. Liq.* **2019**, *294*, 111588. doi:10.1016/j.molliq.2019.111588.

35. Marchel M, Cieśliński H, Boczkaj G. Thermal Instability of Choline Chloride-Based Deep Eutectic Solvents and Its Influence on Their Toxicity-Important Limitations of DESs as Sustainable Materials. *Ind. Eng. Chem. Res.* **2022**, *61*, 11288–11300. doi:10.1021/acs.iecr.2c01898.
36. Chen W, Xue Z, Wang J, Jiang J, Zhao X, Mu T. Investigation on the Thermal Stability of Deep Eutectic Solvents. *Acta Phys. Chim. Sin.* **2018**, *34*, 904–911. doi:10.3866/pku.Whxb201712281.
37. Jahanbakhshi M, Ghaemi A, Helmi M. Impregnation of Silica Gel with Choline Chloride-MEA as an eco-friendly adsorbent for CO2 capture. *Sci. Rep.* **2024**, *14*, 15208. doi:10.1038/s41598-024-66334-0.
38. Bide Y, Fashapoyeh MA, Shokrollahzadeh S. Structural investigation and application of Tween 80-choline chloride self-assemblies as osmotic agent for water desalination. *Sci. Rep.* **2021**, *11*, 17068. doi:10.1038/s41598-021-96199-6.
39. Migliorati V, Sessa F, D'Angelo P. Deep eutectic solvents: A structural point of view on the role of the cation. *Chem. Phys. Lett.* **2019**, *737*, 100001. doi:10.1016/j.cpletx.2018.100001.
40. Di Pietro ME, Tortora M, Bottari C, Colombo Dugoni G, Pivato RV, Rossi B, et al. In Competition for Water: Hydrated Choline Chloride:Urea vs Choline Acetate:Urea Deep Eutectic Solvents. *ACS Sustain. Chem. Eng.* **2021**, *9*, 12262–12273. doi:10.1021/acssuschemeng.1c03811.
41. Rico X, Nuutinen EM, Gullón B, Pihlajaniemi V, Yáñez R. Application of an eco-friendly sodium acetate/urea deep eutectic solvent in the valorization of melon by-products. *Food Bioprod. Process.* **2021**, *130*, 216–228. doi:10.1016/j.fbp.2021.10.006.
42. Takahashi Y. Latent heat measurement by DSC with sapphire as standard material. *Thermochim. Acta* **1985**, *88*, 199–204. doi:10.1016/0040-6031(85)85429-0.
43. Long H, Liao W, Liu R, Zeng R, Li Q, Zhao L. Significantly Improve the Thermal Conductivity and Dielectric Performance of Epoxy Composite by Introducing Boron Nitride and POSS. *Nanomaterials* **2024**, *14*, 205. doi:10.3390/nano14020205.
44. Smith EL, Abbott AP, Ryder KS. Deep Eutectic Solvents (DESs) and Their Applications. *Chem. Rev.* **2014**, *114*, 11060–11082. doi:10.1021/cr300162p.
45. Liu C, Yan Y, Sun W, Shi X, Shi N, Huo Y, et al. Preparation and thermophysical study on a super stable copper oxide/deep eutectic solvent nanofluid. *J. Mol. Liq.* **2022**, *356*, 119020. doi:10.1016/j.molliq.2022.119020.